# Human Presenilin-1 delivered by AAV9 rescues impaired γ-secretase activity, memory deficits, and neurodegeneration in *Psen* mutant mice

Paola Montenegro[a,1] (ID), Phoenix Chen[a] (ID), Jongkyun Kang[a] (ID), Sang Hun Lee[a] (ID), Sofia Leone[a] (ID), and Jie Shen[a,b,2] (ID)

Mutations in the *Presenilin* (*PSEN1* and *PSEN2*) genes are the major cause of early-onset familial Alzheimer's disease (FAD). Presenilin (PS) is the catalytic subunit of the γ-secretase complex, which cleaves type I transmembrane proteins, such as Notch and the amyloid precursor protein (APP), and plays an evolutionarily conserved role in the protection of neuronal survival during aging. FAD *PSEN1* mutations exhibit impaired γ-secretase activity in cell culture, in vitro, and knockin (KI) mouse brains, and the L435F mutation is the most severe in reducing γ-secretase activity and is located closest to the active site of γ-secretase. Here, we report that introduction of the codon-optimized wild-type human *PSEN1* cDNA by adeno-associated virus 9 (AAV9) results in broadly distributed, sustained, low to moderate levels of human PS1 (hPS1) expression and rescues impaired γ-secretase activity in the cerebral cortex of *Psen* mutant mice either lacking PS or expressing the *Psen1* L435F KI allele, as evaluated by endogenous γ-secretase substrates of APP and recombinant γ-secretase products of Notch intracellular domain and Aβ peptides. Furthermore, introduction of hPS1 by AAV9 alleviates impairments of synaptic plasticity and learning and memory in *Psen* mutant mice. Importantly, AAV9 delivery of hPS1 ameliorates neurodegeneration in the cerebral cortex of aged *Psen* mutant mice, as shown by the reversal of age-dependent loss of cortical neurons and elevated microgliosis and astrogliosis. These results together show that moderate hPS1 expression by AAV9 is sufficient to rescue impaired γ-secretase activity, synaptic and memory deficits, and neurodegeneration caused by *Psen* mutations in mouse models.

Alzheimer's disease | gene therapy | learning and memory | synaptic plasticity | gliosis

Alzheimer's disease (AD) is the leading form of dementia, but there is no effective disease-modifying therapy. Mutations in the *Presenilin* (*PSEN*) genes are the major cause of early-onset familial AD (FAD), highlighting the importance of Presenilin (PS) in AD pathogenesis. PS is the catalytic subunit of γ-secretase, an intramembrane protease that cleaves type I transmembrane proteins, including the amyloid precursor protein (APP) and Notch (1). During development, PS regulates neurogenesis through the Notch signaling pathway (2–7). In the adult brain, PS is required for learning and memory, neurotransmitter release, synaptic plasticity, and neuronal survival during aging (8–18). Moreover, partial loss of PS function in excitatory neurons of the postnatal forebrain also results in age-dependent cortical neuronal loss and increases of apoptosis though to a lesser extent and at a later age of onset (16), relative to complete inactivation of PS (11). Furthermore, the essential role of PS in support of neuronal survival in the aging brain is conserved from *Drosophila* to mammals (11, 17). Based on these genetic findings, we proposed the Presenilin hypothesis, which posits that loss of PS essential function underlies neurodegeneration in FAD (19).

*PSEN1* mutations in FAD were reported to show loss of its essential function and γ-secretase activity in cultured cells, knockin (KI) mice, and cell-free systems (20–25). Using a sensitive, quantitative cell culture system to evaluate the effect of *PSEN1* mutations on γ-secretase activity, we found that all mutations tested result in partial to near complete loss of γ-secretase activity with the L435F mutation causing the most dramatic loss of γ-secretase activity and that mutant PS1 exerts a dominant negative effect and inhibits γ-secretase activity of wild-type PS1 in trans (20, 21). Strikingly, both homozygous *Psen1* L435F and C410Y KI/KI mice exhibit phenotypes that resemble *Psen1*−/− mice, including perinatal lethality, neurogenesis impairment, reduced Notch signaling, and undetectable γ-secretase activity and Aβ production (22, 23). Furthermore, the L435F KI allele results in synaptic and memory impairments and age-dependent neurodegeneration, similar to those caused by complete inactivation of PS (11, 22). Subsequent structural analysis placed the side chain of the L435 residue between D257 and D385, the two aspartate residues that constitute the active site of γ-secretase (26), providing an independent structural explanation for the

## Significance

Alzheimer's disease (AD) is the most common neurodegenerative disorder, but there is no effective disease-modifying therapy, despite substantial efforts from major pharmaceutical companies targeting amyloid peptides. In contrast to the prevailing amyloid hypothesis, the Presenilin hypothesis posits that impairment of Presenilin function or γ-secretase activity drives neurodegeneration and dementia in familial AD. The current multidisciplinary study provides preclinical proof-of-concept data showing that introduction of a wild-type human *PSEN1* cDNA by adeno-associated virus 9 rescues impaired γ-secretase activity, synaptic and memory deficits, loss of cortical neurons, microgliosis, and astrogliosis caused by *Psen* mutations in mice.

severe loss of function phenotypes exhibited by L435F. Furthermore, large biochemical studies of 138 *PSEN1* mutations showed that ~90% of mutations cause loss of γ-secretase activity with ~30% of mutations abolishing its activity (24, 25). Last, human neurons derived from isogenic iPS cells carrying FAD *PSEN1* ΔE9 (exon 9 deletion) or wild-type *PSEN1* allele demonstrated that *PSEN1* ΔE9 results in decreases of γ-secretase activity (27).

In the current study, we test whether introduction of wild-type human PS1 (hPS1) rescues impairment of γ-secretase activity, synaptic and memory deficits, and neurodegeneration in *Psen* mutant mice. We found that despite low to moderate levels of hPS1 expressed from the AAV9 vector, hPS1 expression is sustained over time and rescues impaired γ-secretase activity in the cerebral cortex of *Psen* mutant mice either lacking PS or expressing *Psen1* L435F, as shown by the reversal of accumulation of γ-secretase substrates, APP C-terminal fragments (CTFs), and by the restored de novo production of amyloid peptides and the Notch intracellular domain (NICD). Furthermore, introduction of hPS1 alleviates impaired hippocampal synaptic plasticity and memory deficits exhibited by *Psen* mutant mice. Importantly, hPS1 expression ameliorates neurodegeneration in aged *Psen* mutant mice. These results together demonstrate that hPS1 introduced by AAV9 successfully rescued impaired γ-secretase activity, synaptic and memory deficits, and neurodegeneration caused by *Psen* mutations in mouse models.

## Results

### AAV9 Delivery of hPS1 Rescues Impaired γ-secretase Activity in *Psen* Mutant Mice.
To introduce wild-type hPS1 into mouse models bearing various *Psen* mutations, we generated three recombinant AAV vectors expressing hPS1 together with EGFP separated by the T2A peptide, hPS1 alone, or EGFP alone under the control of the human *Camk2a* promoter (Fig. 1A). The T2A peptide (21 amino acid residues) enables separation of hPS1 and EGFP by ribosomal skip (28), thus labeling cells that are transduced by *AAV9/hPS1-EGFP*. A chimeric intron and the late *SV40* polyA sequences were also included to optimize mRNA expression and stabilization. We selected neurotropic AAV serotype 9 for its broad transduction in the central nervous system (29). The *Camk2a* promoter was chosen because of its robust expression in excitatory neurons of the postnatal cerebral cortex (30), where *Psen1* is highly expressed (8, 11, 12).

To determine whether delivery of hPS1 by AAV9 restores impaired γ-secretase activity, we first used the most dramatic *Psen* mutant mice, *PS* conditional double knockout (cDKO), in which PS is inactivated selectively in excitatory neurons of the postnatal forebrain, as they exhibit a robust reduction of γ-secretase activity and age-dependent neurodegeneration (8, 9, 11, 13). *AAV9/hPS1-EGFP* or *AAV9/EGFP* (3 μL, $4 \times 10^{10}$ gc) was injected into intracerebral ventricles of *PS* cDKO mice and littermate controls at postnatal day 0 (P0). Western analysis showed the expected reduction of mouse PS1 (mPS1) CTF in the cortex of *PS* cDKO mice at 2 mo of age (*SI Appendix*, Fig. S1 *A* and *B*). The remaining mPS1 CTF (~50%) detected in the cortex of *PS* cDKO mice is due to the normal mPS1 expression in inhibitory neurons and glial populations that are not targeted by the Cre line (8, 11, 12, 14). Injection of *AAV9/hPS1-EGFP* but not *AAV9/EGFP* results in an additional larger band, of approximately 22kDa, corresponding to the T2A-tagged hPS1 CTF following ribosomal skip, which includes 18 amino acid residues of the T2A peptide attached
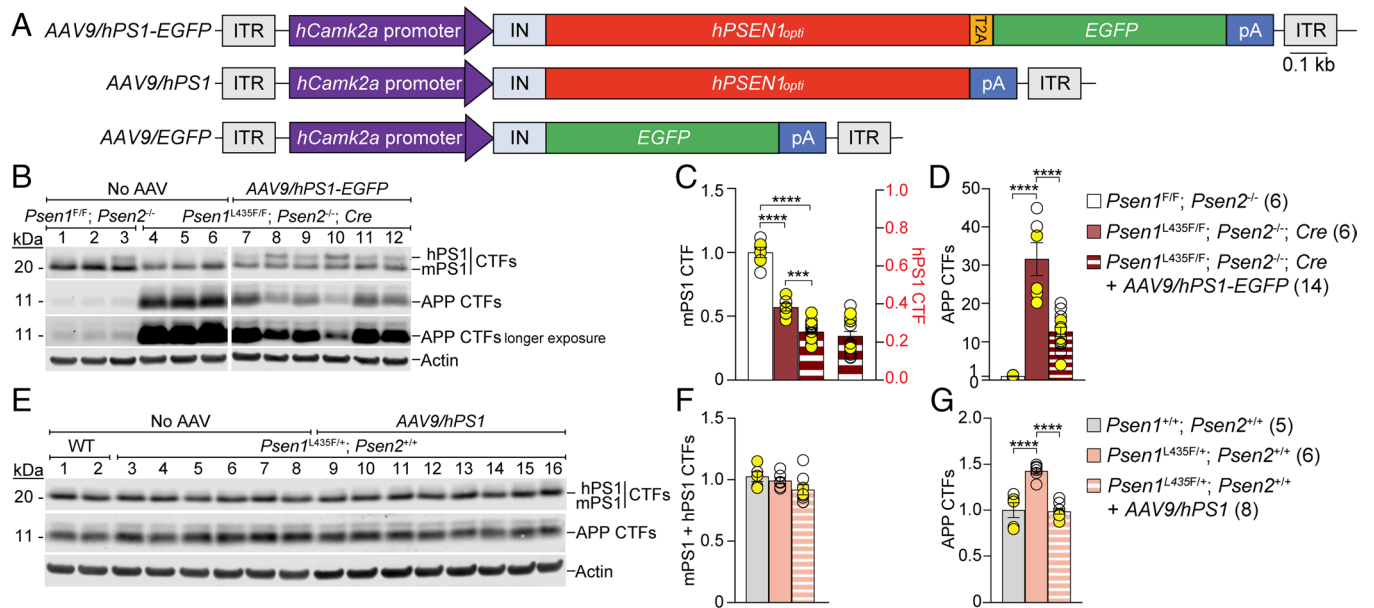


**Fig. 1.** AAV9 delivery of hPS1 reverses APP CTF accumulation in *Psen* mutant mice. (*A*) Schematic illustration of *AAV9/hCamk2a-hPSEN1*$_{opti}$*-T2A-EGFP* (*AAV9/hPS1-EGFP*), *AAV9/hCamk2a-hPSEN1*$_{opti}$ (*AAV9/hPS1*), *AAV9/hCamk2a-EGFP* (*AAV9/EGFP*) vectors. The codon-optimized human *PSEN1* cDNA (*hPSEN1*$_{opti}$), the *EGFP* cDNA, or both cDNAs together with *T2A* is expressed under the control of the human *Camk2a* promoter. A chimeric intron (IN) from human *β-globin* and *immunoglobulin heavy chain* and the late *SV40* polyA (pA) are also included. (*B–D*) Expression of hPS1 by *AAV9/hPS1-EGFP* reduces levels of mPS1 CTF and rescues accumulation of APP CTFs in *Psen1*$^{L435F/F}$; *Psen2*$^{−/−}$; *Cre* mice. (*B*) Western analysis of cortical lysates shows a reduction of mPS1 CTF in *Psen1*$^{L435F/F}$; *Psen2*$^{−/−}$; *Cre* mice (Lanes 4-6), compared to controls (Lanes 1-3), and expression of varying levels of hPS1 CTF (slightly larger due to the 18 aa derived from cleaved T2A) in *AAV9/hPS1-EGFP*-injected cortices (Lanes 7-12). Western analysis also shows a dramatic accumulation of APP CTFs in *Psen1*$^{L435F/F}$; *Psen2*$^{−/−}$; *Cre* mice (Lanes 4-6), compared to littermate controls (Lanes 1-3), and varying levels of reduction of APP CTFs in *AAV9/hPS1-EGFP*-injected cortices (Lanes 7-12). Higher levels of hPS1 correlate with lower levels of APP CTF accumulation (e.g., Lanes 8, 10). Quantification of mPS1 and hPS1 CTFs (*C*) and APP CTFs (*D*) shows that levels of mPS1 CTF are significantly reduced in *AAV9/hPS1-EGFP*-injected *Psen1*$^{L435F/F}$; *Psen2*$^{−/−}$; *Cre* mice, compared to uninjected (*P* = 0.0002), and that *AAV9/hPS1-EGFP* dramatically reduces the accumulation of APP CTFs in *Psen1*$^{L435F/F}$; *Psen2*$^{−/−}$; *Cre* mice, compared to uninjected (*P* < 0.0001). (*E–G*) *AAV9/hPS1* restores levels of APP CTFs in the cerebral cortex of *Psen1*$^{L435F/+}$ mice. (*E*) Western analysis shows combined mPS1 and hPS1 CTFs, due to the lack of T2A in *AAV9/hPS1*, and APP CTFs. Quantification of mPS1 and hPS1 CTFs (*F*) and APP CTFs (*G*) shows that levels of APP CTFs are significantly increased in the cortex of *Psen1*$^{L435F/+}$; *Psen2*$^{+/+}$ mice, compared to control mice (*P* < 0.0001), and that *AAV9/hPS1* restores levels of APP CTFs in *Psen1*$^{L435F/+}$; *Psen2*$^{+/+}$ mice (*P* < 0.0001). All data represent mean ± SEM. ***P* < 0.001, *****P* < 0.0001. Yellow filled and open circles represent data obtained from individual male and female mice, respectively.

to the PS1 CTF (*SI Appendix,* Fig. S1*A*). Levels of the hPS1 CTF vary (5 to 36%) in the cortex of individual *AAV9/hPS1-EGFP*-injected *PS* cDKO mice, compared to levels of mPS1 CTF in control mice. Furthermore, immunohistochemical analysis of the cerebral cortex of *PS* cDKO mice injected with *AAV9/hPS1-EGFP* showed that GFP immunoreactivity colocalizes with NeuN, indicating broad distribution of *AAV9/hPS1-EGFP* delivery (*SI Appendix,* Fig. S2*A*). There is no detected colocalization between GFP and GFAP or Iba1, markers of astrocytes or microglia, respectively, suggesting the specificity of hPS1 expression in neurons (*SI Appendix,* Fig. S2 *B* and *C*). We then examined the effect of hPS1 expression by *AAV9/hPS1-EGFP* on endogenous APP CTFs, which are substrates of γ-secretase. We previously reported accumulation of APP CTFs in the cortex of *PS* cDKO mice (9). Indeed, levels of APP CTFs in the cortex of *PS* cDKO mice are greatly elevated ($P < 0.0001$, *SI Appendix,* Fig. S1 *A and C*). *AAV9/hPS1-EGFP* results in drastic decreases of APP CTFs in *PS* cDKO mice ($P < 0.0001$), whereas *AAV9/EGFP* has no effect ($P = 0.9966$, *SI Appendix,* Fig. S1*C*). Furthermore, *AAV9/hPS1-EGFP* but not *AAV9/EGFP* reverses high levels of APP CTF immunoreactivity in the cortex of *PS* cDKO mice (*SI Appendix,* Fig. S3).

We then examined the effect of hPS1 on FAD *PSEN1* mutations, and we chose the severe mutation L435F (20, 22, 23, 25, 26). *AAV9/hPS1-EGFP* was introduced into *Psen1*$^{L435F/F}$; *Psen2*$^{-/-}$; *Cre* mice, and Western blotting showed a significant reduction of mPS1 CTF in the cortex of *Psen1*$^{L435F/F}$; *Psen2*$^{-/-}$; *Cre* mice, compared to controls ($P < 0.0001$, Fig. 1 *B* and *C*). Interestingly, levels of mPS1 CTF in the cortex of *AAV9/hPS1-EGFP*-injected *Psen1*$^{L435F/F}$; *Psen2*$^{-/-}$; *Cre* mice are further reduced, compared to uninjected *Psen1*$^{L435F/F}$; *Psen2*$^{-/-}$; *Cre* mice ($P = 0.0002$, Fig. 1*C*), suggesting a displacement of L435F mutant mPS1 by hPS1. Expression of hPS1 by *AAV9/hPS1-EGFP* (12-39%, compared to control mice) in *Psen1*$^{L435F/F}$; *Psen2*$^{-/-}$; *Cre* mice results in drastic reduction of APP CTFs, compared to uninjected mice ($P < 0.0001$, Fig. 1*D*), indicating that hPS1 restores impaired γ-secretase activity in these mutant mice.

We further evaluated the effect of *AAV9/hPS1-EGFP* on γ-secretase activity in *Psen1*$^{L435F/+}$; *Psen2*$^{-/-}$ mice (*SI Appendix,* Fig. S1 *D–F*). Injection of higher amounts ($7 \times 10^{10}$ gc) gave rise to higher levels of hPS1 expression (32 to 79% relative to mPS1 CTF levels in control mice). We observed a significant increase in APP CTFs in the cortex of *Psen1*$^{L435F/+}$; *Psen2*$^{-/-}$ mice, compared to littermate controls ($P < 0.0001$), and *AAV9/hPS1-EGFP* results in a significant reduction of APP CTFs, compared to uninjected mice ($P = 0.0001$). We further examined the effect of *AAV9/hPS1* on *Psen1*$^{L435F/+}$ mice, which are genetically identical to FAD patients carrying the same mutation (Fig. 1 *E–G*). Western analysis shows a significant increase of APP CTFs in the cortex of *Psen1*$^{L435F/+}$; *Psen2*$^{+/+}$ mice, compared to littermate wild-type controls ($P < 0.0001$), and *AAV9/hPS1* significantly reduces levels of APP CTFs, compared to uninjected mice ($P < 0.0001$, Fig. 1*G*). These results together showed that AAV9 delivery of hPS1 by *AAV9/hPS1-EGFP* or *AAV9/hPS1* is distributed broadly in the cerebral cortex and restores impaired γ-secretase activity by reversing accumulation of γ-secretase substrates APP CTFs in four sets of *Psen* mutant mice, from *PS* cDKO to the FAD equivalent *Psen1* L435F KI/+ mice.

We further evaluated γ-secretase activity directly employing a well-established in vitro γ-secretase assay using CHAPSO solubilized membrane fractions from dissected cortices, which retain γ-secretase activity while using recombinant Notch and APP substrates (31, 32). Using a recombinant Notch substrate N102-FmH followed by Western analysis, we found that production of NICD is significantly reduced (–49%) using cortical membrane fractions from *Psen1*$^{L435F/+}$; *Psen2*$^{-/-}$ mice, compared

to littermate *Psen1*$^{+/+}$; *Psen2*$^{-/-}$ controls ($P = 0.0022$; *SI Appendix,* Fig. S4*A*). Expression of hPS1 delivered by *AAV9/hPS1* rescues impaired NICD production in *Psen1*$^{L435F/+}$; *Psen2*$^{-/-}$ mice ($P = 0.0247$, *SI Appendix,* Fig. S4*A*). Similarly, production of NICD is significantly reduced (–49%) using cortical membrane fractions from *Psen1*$^{L435F/+}$; *Psen2*$^{+/+}$ mice, compared to littermate wild-type controls ($P = 0.0005$), and *AAV9/hPS1* significantly rescues impaired NICD production in *Psen1*$^{L435F/+}$; *Psen2*$^{+/+}$ injected L435F KI/+ mice ($P = 0.0003$, *SI Appendix,* Fig. S4*C*). Using a recombinant APP substrate C99 followed by ELISA measurements of Aβ40 and Aβ42, we found significant decreases of Aβ40 (–42%, $P = 0.0001$) and Aβ42 (–34%, $P = 0.0171$) production using cortical membrane fractions from *Psen1*$^{L435F/+}$; *Psen2*$^{-/-}$ mice (*SI Appendix,* Fig. S4*B*). *AAV9/hPS1* restores the production of Aβ40 ($P = 0.0024$) and Aβ42 ($P = 0.0014$) in *Psen1*$^{L435F/+}$; *Psen2*$^{-/-}$ mice. Similarly, Aβ40 production is markedly reduced (–51%) in *Psen1*$^{L435F/+}$; *Psen2*$^{+/+}$ mice, compared to controls ($P = 0.0069$), and *AAV9/hPS1* rescues Aβ40 production ($P = 0.0043$, *SI Appendix,* Fig. S4*D*).

**AAV9 Delivery of hPS1 Alleviates Synaptic and Memory Impairments in *Psen* Mutant Mice.** PS is required for hippocampal synaptic plasticity and learning and memory, and the L435F mutation impairs long-term potentiation (LTP) in the Schaffer collateral (SC) pathway and spatial long-term memory in the water maze task (11, 12, 14, 15, 18, 22, 33). To determine whether hPS1 rescues synaptic and memory deficits exhibited by *Psen* mutant mice, we performed electrophysiological analysis in the hippocampal SC pathway of *AAV9/hPS1-EGFP*-injected *PS* cDKO mice at 2 mo of age compared to *AAV9/EGFP*-injected control and *PS* cDKO mice. Paired-pulse facilitation (PPF), a form of presynaptic short-term plasticity, is significantly reduced in *PS* cDKO mice, compared to littermate controls ($F_{1,18} = 36.83$, $P < 0.0001$; *SI Appendix,* Fig. S5*A*). *AAV9/hPS1-EGFP* significantly enhanced PPF in *PS* cDKO mice, compared to *AAV9/EGFP* ($F_{1,24} = 26.02$; $P < 0.0001$, *SI Appendix,* Fig. S5*A*). Similarly, synaptic facilitation, elicited at 10 or 20 Hz, is impaired in *AAV9/EGFP*-injected *PS* cDKO mice, and *AAV9/hPS1-EGFP* fully rescued the deficits in *PS* cDKO mice (*SI Appendix,* Fig. S5*B*). Furthermore, LTP induced by five trains of *theta* burst stimulation (TBS) is impaired in the SC pathway of *PS* cDKO mice, and *AAV9/hPS1-EGFP* reversed LTP deficits ($P = 0.0067$; *SI Appendix,* Fig. S5*C*). Short-term (PPF, synaptic facilitation) and LTP induction are normal in the SC pathway of control mice injected with *AAV9/hPS1*-EGFP, compared to *AAV9/EGFP* (*SI Appendix,* Fig. S6).

We further examined whether hPS1 rescues learning and memory deficits exhibited by *Psen* mutant mice using a relatively challenging training protocol in the hidden platform of the water maze (4 trials a day for 12 d, probe trials after 6 and 12 d of training). Both *PS* cDKO mice injected with *AAV9/EGFP* ($F_{1,24} = 121.1$, $P < 0.0001$, two-way ANOVA) and *Psen1*$^{L435F/F}$; *Psen2*$^{-/-}$; *Cre* mice injected with *AAV9/EGFP* or no AAV ($F_{1,20} = 64.77$, $P < 0.0001$) exhibited longer escape latencies, compared to the control group (Fig. 2*A*). Compared to the control AAV group, *AAV9/hPS1-EGFP* rescued the delayed latency of *PS* cDKO mice ($F_{1,21} = 51.27$, $P < 0.0001$) and *Psen1*$^{L435F/F}$; *Psen2*$^{-/-}$; Cre mice ($F_{1,12} = 8.42$, $P = 0.0133$). All 5 groups significantly improved their performance during 12 d of training ($P < 0.0001$).

In the posttraining probe trial on day 13, *PS* cDKO mice injected with *AAV9/EGFP* showed significantly reduced target quadrant occupancy ($P < 0.0001$) and platform crossing ($P < 0.0001$), compared to control mice (Fig. 2*B*). *AAV9/hPS1-EGFP* significantly increased the number of platform crossing exhibited by *PS* cDKO mice in the target quadrant, relative to *AAV9/EGFP*
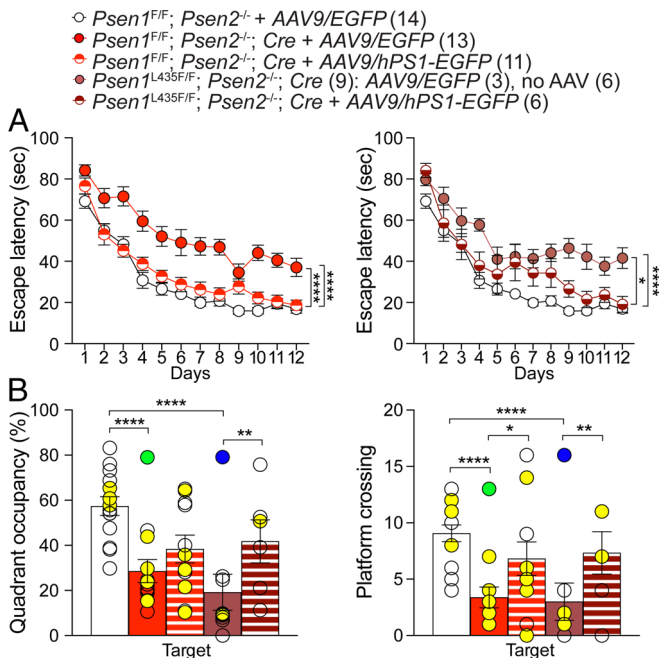
- ○ *Psen1*<sup>F/F</sup>; *Psen2*<sup>-/-</sup> + AAV9/EGFP (14)
- ● *Psen1*<sup>F/F</sup>; *Psen2*<sup>-/-</sup>; Cre + AAV9/EGFP (13)
- ● *Psen1*<sup>F/F</sup>; *Psen2*<sup>-/-</sup>; Cre + AAV9/hPS1-EGFP (11)
- ● *Psen1*<sup>L435F/F</sup>; *Psen2*<sup>-/-</sup>; Cre (9): AAV9/EGFP (3), no AAV (6)
- ● *Psen1*<sup>L435F/F</sup>; *Psen2*<sup>-/-</sup>; Cre + AAV9/hPS1-EGFP (6)

**Fig. 2.** AAV9 delivery of hPS1 improves spatial learning and memory deficits in *Psen* mutant mice. (*A*) In the hidden platform version of the water maze test, *AAV9/EGFP*-injected *PS* cDKO mice at ~5 mo of age display significantly longer latencies, compared to littermate controls ($F_{1,24} = 121.1$, $P < 0.0001$, two-way ANOVA with Bonferroni's post hoc multiple comparisons). *AAV9/hPS1-EGFP* injection rescues the delayed latency of *PS* cDKO mice, compared to *AAV9/EGFP* ($F_{1,21} = 51.27$, $P < 0.0001$). Similarly, *Psen1*<sup>L435F/F</sup>; *Psen2*<sup>-/-</sup>; *Cre* mice also display significantly longer latencies, compared to the control group ($F_{1,20} = 64.77$, $P < 0.0001$), and *AAV9/hPS1-EGFP* significantly improves the longer latency of these mutant mice ($F_{1,12} = 8.42$, $P = 0.0133$). Note, the same littermate control group is shown in both latency graphs for better visual comparison with *Psen* mutant groups. The performance of all five groups improved significantly during the training course (days 1 vs. 12: $P < 0.0001$, two-way ANOVA with Tukey's post hoc multiple comparisons). (*B*) In the posttraining probe trial, *AAV9/EGFP*-injected *PS* cDKO mice exhibit significantly reduced target quadrant occupancy ($P < 0.0001$, one-way ANOVA with Tukey's post hoc multiple comparisons) and platform crossing ($P < 0.0001$), compared to control mice. *AAV9/hPS1-EGFP* significantly improves target platform crossing in *PS* cDKO mice, compared to *AAV9/EGFP* ($P = 0.0119$). Similarly, *Psen1*<sup>L435F/F</sup>; *Psen2*<sup>-/-</sup>; *Cre* mice also show significantly reduced target quadrant occupancy ($P < 0.0001$) and platform crossing ($P < 0.0001$), compared to control mice. *AAV9/hPS1-EGFP* significantly improves target quadrant occupancy ($P = 0.0050$) and platform crossing ($P = 0.0026$), compared to uninjected or control AAV injected *Psen1*<sup>L435F/F</sup>; *Psen2*<sup>-/-</sup>; *Cre* mice. Green and blue filled circles represent statistical outliers identified by ROUT method Q = 1%, which were excluded from statistical analysis. All data represent mean ± SEM. *$P < 0.05$, **$P < 0.01$, ****$P < 0.0001$. Yellow filled and open circles represent data obtained from individual male and female mice, respectively.

($P = 0.0119$, Fig. 2*B*). Similarly, *Psen1*<sup>L435F/F</sup>; *Psen2*<sup>-/-</sup>; *Cre* mice displayed lower target quadrant occupancy ($P < 0.0001$) and platform crossing ($P < 0.0001$), compared to the control group, and introduction of *AAV9/hPS1-EGFP* resulted in significant increases in target quadrant occupancy ($P = 0.0050$) and platform crossing ($P = 0.0026$, Fig. 2*B*). All five groups performed similarly in the visible platform version of the water maze task (*SI Appendix*, Fig. S7). Western analysis of dissected cortices following the completion of the water maze test confirmed continued expression of hPS1 at this age (~6 mo) and decreases of APP CTFs in individual *AAV9/hPS1-EGFP*-injected but not *AAV9/EGFP*-injected *Psen* mice (*SI Appendix*, Fig. S8A).

**hPS1 Delivered by AAV9 Ameliorates Cortical Neurodegeneration in *Psen* Mutant Mice.** Previous studies showed that *Psen* mutant mice, either lacking PS or carrying the FAD mutation *Psen1* L435F, exhibit age-dependent neuronal loss and gliosis (9, 11, 13, 16, 22). To determine the impact of hPS1 expression delivered

by AAV9 on neuronal survival in *Psen* mutant mice, we performed histological analysis of *PS* cDKO, *Psen1*<sup>L435F/F</sup>; *Psen2*<sup>-/-</sup>; *Cre*, and littermate control mice at 10 mo of age either injected with *AAV9/hPS1-EGFP* or no AAV (Fig. 3*A*). Stereological quantification shows that the number of NeuN+ neurons in the neocortex of *PS* cDKO mice is markedly reduced (-35%), compared to littermate controls ($P < 0.0001$) and that the number of NeuN+ neurons in the neocortex of *Psen1*<sup>L435F/F</sup>; *Psen2*<sup>-/-</sup>; *Cre* mice is also significantly reduced ($P < 0.0001$, one-way ANOVA with Tukey's multiple comparison test, Fig. 3*B*). *AAV9/hPS1-EGFP* injection restores the loss of cortical neurons in *PS* cDKO mice ($P < 0.0001$), and the number of cortical neurons in *AAV9/hPS1-EGFP*-injected *PS* cDKO mice is similar to that in littermate controls ($P = 0.1122$, Fig. 3*B*). Similarly, *AAV9/hPS1-EGFP* also restores the loss of cortical neurons in *Psen1*<sup>L435F/F</sup>; *Psen2*<sup>-/-</sup>; *Cre* mice ($P = 0.0003$), and the number of cortical neurons is similar between *AAV9/hPS1-EGFP*-injected *Psen1*<sup>L435F/F</sup>; *Psen2*<sup>-/-</sup>; *Cre* mice and control mice ($P = 0.3270$).

Microgliosis often accompanies neurodegeneration (34, 35). We therefore performed immunohistochemical analysis of Iba1, a microglial marker, and found that the number of Iba1+ microglia is significantly higher in the neocortex and hippocampus of *PS* cDKO mice at 10 mo of age, compared to littermate controls ($P < 0.0001$, Fig. 4 *A* and *B*). The number of Iba1+ microglia is also higher in the neocortex ($P < 0.0001$) and hippocampus ($P = 0.0001$) of *Psen1*<sup>L435F/F</sup>; *Psen2*<sup>-/-</sup>; *Cre* mice (Fig. 4 *A* and *B*). *AAV9/hPS1-EGFP* reduced the number of Iba1+ cells in the neocortex and hippocampus of *PS* cDKO mice ($P < 0.0001$) and *Psen1*<sup>L435F/F</sup>; *Psen2*<sup>-/-</sup>; *Cre* mice ($P < 0.0001$; Fig. 4 *A* and *B*). We further quantified the number and percentage of microglia in their most activated state based on their amoeboid morphology (*SI Appendix*, Fig. S9A). The number of amoeboid microglia is drastically elevated in the cortex of *PS* cDKO mice ($P < 0.0001$) and *Psen1*<sup>L435F/F</sup>; *Psen2*<sup>-/-</sup>; *Cre* mice ($P < 0.0001$), and *AAV9/hPS1-EGFP* restores the number of amoeboid microglia in these *Psen* mutant mice ($P < 0.0001$; *SI Appendix*, Fig. S9B).

We previously reported elevated astrogliosis in the cerebral cortex of *PS* cDKO mice at 6 mo of age and *Psen1*<sup>L435F/F</sup>; *Psen2*<sup>-/-</sup>; *Cre* mice at 12 mo of age, accompanied with neuronal loss (9, 22). As expected, levels of GFAP, a marker of astrocytes, are elevated in the cortex of *PS* cDKO mice ($P < 0.0001$) and *Psen1*<sup>L435F/F</sup>; *Psen2*<sup>-/-</sup>; *Cre* mice ($P < 0.0001$) at 10 mo of age, compared to littermate controls (Fig. 4 *C* and *D*). *AAV9/hPS1-EGFP* injection restores levels of GFAP in the cortex of *PS* cDKO ($P < 0.0001$) and *Psen1*<sup>L435F/F</sup>; *Psen2*<sup>-/-</sup>; *Cre* mice ($P < 0.0001$, Fig. 4 *C* and *D*). We further performed GFAP immunostaining and quantified GFAP-immunoreactive areas in the cortex (*SI Appendix*, Fig. S10A). Consistent with GFAP levels measured by immunoblotting, GFAP-immunoreactive areas are dramatically elevated in the cortex of *Psen* mutant mice, and *AAV9/hPS1-EGFP* reverses astrogliosis in these *Psen* mutant mice (*SI Appendix*, Fig. S10B). Western analysis of dissected cortices from the same brains used in neuropathological studies (one hemisphere for each analysis) confirmed continued expression of hPS1 at this age (~10 mo) and decreases of APP CTFs in individual *AAV9/hPS1-EGFP*-injected *Psen* mice (*SI Appendix*, Fig. S8B). Furthermore, GFP and NeuN immunostaining showed sustained, broadly distributed GFP expression in NeuN+ neurons in the neocortex and hippocampus of *AAV9/hPS1-EGFP*-injected *PS* cDKO mice at 10 mo of age (*SI Appendix*, Fig. S11).

Together, these findings demonstrate that *AAV9/hPS1-EGFP* delivers sustained hPS1 expression in the aged cerebral cortex and achieves reversal of APP CTF accumulation broadly in the cortex and that low to moderate levels of hPS1 expression are able to
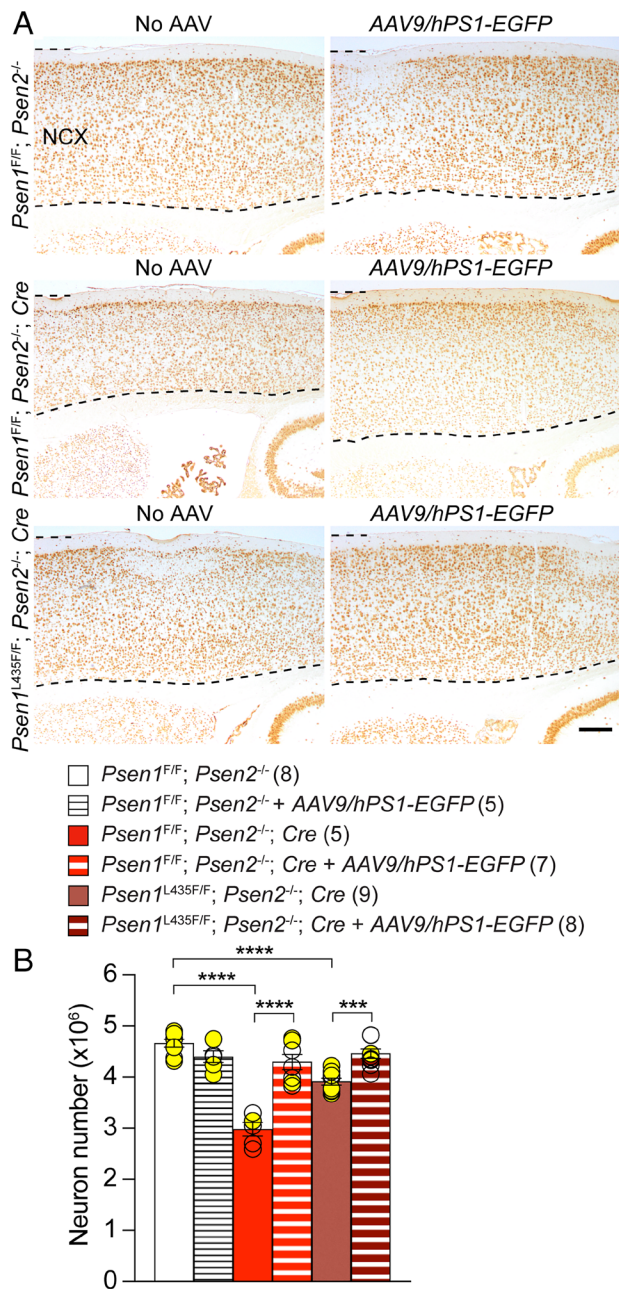
**Fig. 3.** AAV9 delivery of hPS1 rescues cortical neuronal loss in *Psen* mutant mice. (*A*) *AAV9/hPS1-EGFP* restores loss of cortical neurons in *PS* cDKO and *Psen1*[L435F/F]; *Psen2*^{−/−}; *Cre* mice at ~10 mo of age. Immunohistochemical analysis of NeuN shows that the neocortex (NCX) of *PS* cDKO and *Psen1*[L435F/F]; *Psen2*^{−/−}; *Cre* mice injected with *AAV9/hPS1-EGFP* appears thicker, compared to uninjected respective mutant mice. (*B*) Quantitative analysis using stereological methods shows that the number of NeuN+ neurons in the neocortex of *PS* cDKO mice ($2.98 \pm 0.13 \times 10^6$) is significantly reduced, compared to control mice ($4.66 \pm 0.08 \times 10^6$, $P < 0.0001$, one-way ANOVA with Tukey's post hoc multiple comparisons) and that *AAV9/hPS1-EGFP* rescues the loss of cortical neurons in *PS* cDKO mice (injected vs. uninjected, $P < 0.0001$). The number of NeuN+ cortical neurons is similar between *AAV9/hPS1-EGFP*-injected *PS* cDKO mice ($4.30 \pm 0.15 \times 10^6$) and control mice ($P = 0.1122$) or *AAV9/hPS1-EGFP*-injected control mice ($4.40 \pm 0.11 \times 10^6$; $P = 0.9358$). The number of NeuN+ cortical neurons in *Psen1*[L435F/F]; *Psen2*^{−/−}; *Cre* mice ($3.91 \pm 0.07 \times 10^6$) is also significantly reduced, compared to control mice ($P < 0.0001$), and *AAV9/hPS1-EGFP* rescues the reduction of cortical neurons in *Psen1*[L435F/F]; *Psen2*^{−/−}; *Cre* mice (injected vs. uninjected, $P = 0.0003$). The number of cortical neurons is similar between *AAV9/hPS1-EGFP*-injected *Psen1*[L435F/F]; *Psen2*^{−/−}; *Cre* mice ($4.46 \pm 0.09 \times 10^6$) and control mice ($4.66 \pm 0.08 \times 10^6$; $P = 0.3270$) or *AAV9/hPS1-EGFP*-injected control mice ($4.40 \pm 0.11 \times 10^6$; $P = 0.9637$). (Scale bar: 500 μm.) All data represent mean ± SEM. ***$P < 0.001$, ****$P < 0.0001$. Yellow filled and open circles represent data obtained from individual male and female mice, respectively.

alleviate neurodegeneration as well as microgliosis and astrogliosis in aged *Psen* mutant mice.

## Discussion

More than 300 mutations in the *PSEN1* gene have been reported, and highly penetrant mutations in *PSEN1* are the most common cause of early-onset AD (https://www.alzforum.org/mutations/psen-1). Thus, using gene therapy to deliver a functional copy of *PSEN1* to correct dysfunction caused by *PSEN* mutations appears a logical, attractive therapeutic solution. AAVs are considered a promising carrier for delivering transgenes because of their neuronal tropism, stable transgene expression, and low immune responses, and the AAV9 serotype is particularly attractive for gene therapy of CNS disorders due to its ability to achieve widespread gene expression in the CNS (36). In the current study, we perform a preclinical test to determine whether AAV9 delivery of human wild-type PS1 to the brain of a variety of *Psen* mutant mice can rescue impaired γ-secretase activity, synaptic and memory deficits, and neuronal degeneration in the cerebral cortex through the development of three complementary AAV9 vectors expressing either hPS1 together with EGFP to mark transduced cells (*AAV9/hPS1-EGFP*), hPS1 alone (*AAV9/hPS1*), or EGFP alone as control (*AAV9/EGFP*). We found that introduction of *AAV9/hPS1-EGFP* to four different sets of *Psen* mutant mice all rescued impaired γ-secretase activity, as shown by the reversal of accumulation of APP CTFs, best characterized physiological substrates of γ-secretase, in the cerebral cortex of *Psen* mutant mice (Fig. 1 and *SI Appendix*, Figs. S1, S3, S8, and S11). Through examination of γ-secretase activity directly using recombinant Notch or APP substrates, we found that *AAV9/hPS1* also restored decreases of γ-secretase activity in the cerebral cortex of *Psen1* L435F KI/+ mice, which are genetically analogous to FAD patients carrying the same mutation (*SI Appendix*, Fig. S4). Furthermore, introduction of hPS1 alleviates short-term and long-term synaptic plasticity impairments (*SI Appendix*, Figs. S5 and S6) and memory deficits (Fig. 2) exhibited by *Psen* mutant mice. Last, *AAV9/hPS1-EGFP* rescues cortical neurodegeneration in aged *Psen* mutant mice, as shown by the reversal of cortical neuronal loss (Fig. 3) and elevated microgliosis and astrogliosis (Fig. 4 and *SI Appendix*, Figs. S9 and S10) in the cerebral cortex. These results demonstrate that hPS1 introduced by AAV9 reverses impaired γ-secretase activity, synaptic and memory deficits, and neurodegeneration caused by *Psen* mutations in mouse models, providing preclinical proof-of-concept animal data for the use of gene therapy for FAD patients bearing *PSEN* mutations.

**Low to Moderate hPS1 Expression Is Sufficient to Rescue Phenotypes Exhibited by *Psen* Mutant Mice.** APP is perhaps the most sensitive substrate for varying levels of γ-secretase activity, and inactivation of PS results in accumulation of high levels of APP CTFs in the cerebral cortex of *PS* cDKO mice even at 2 mo of age (9). Thus, assessing levels of APP CTFs is a good indicator of γ-secretase activity in cell populations normally expressing APP, which is predominantly expressed in excitatory neurons of the cerebral cortex, as indicated by an 80% reduction of APP in the dissected cortex of excitatory neuron-specific *APP* cKO mice (37). Indeed, introduction of *AAV9/hPS1-EGFP* results in a drastic reversal of APP CTF accumulation in the cortex of *PS* cDKO mice, even though the detected level of hPS1 is quite low, compared to mPS1 in control mice (Fig. 1 and *SI Appendix*, Fig. S1). These results suggest that hPS1 delivered by *AAV9/hPS1-EGFP* is broadly expressed in the cerebral cortex and that low levels of hPS1 are sufficient to rescue the loss of γ-secretase activity
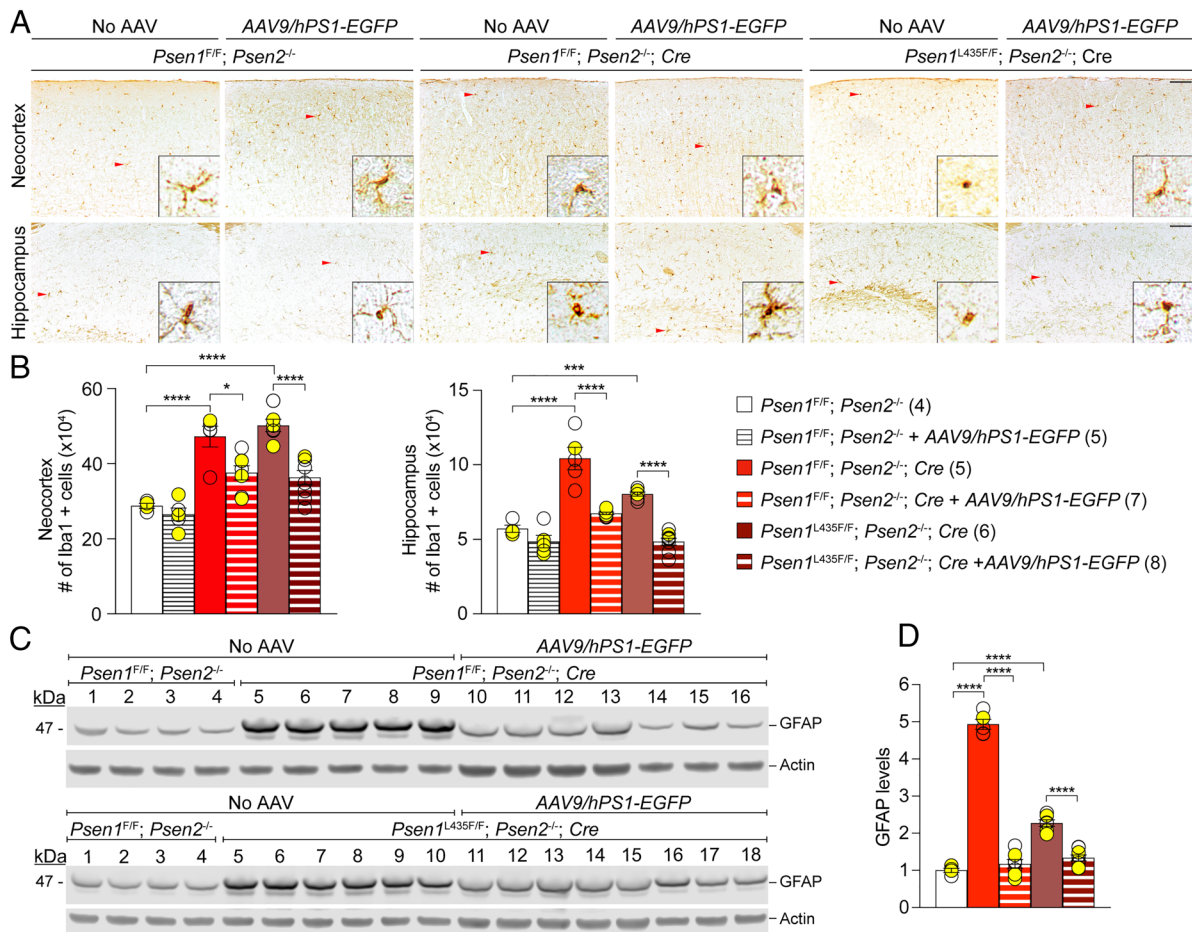
**Fig. 4.** AAV9 delivery of hPS1 reduces elevated gliosis in the cerebral cortex of *Psen* mutant mice. (*A*) Representative images of Iba1 immunoreactivity in the neocortex (NCX) and hippocampus (HP) of littermate *PS* cDKO, *Psen1*[L435F/F]; *Psen2*^{−/−}; *Cre*, and control mice injected with *AAV9/hPS1-EGFP* or no AAV. (Scale bar: 200 μm.) (*B*) Quantification of Iba1+ microglia shows that the number of microglia is significantly elevated in the neocortex ($47.22 \pm 2.77 \times 10^4$) and hippocampus ($10.42 \pm 0.75 \times 10^4$) of *PS* cDKO mice at 10 mo of age, compared to controls (NCX: $28.80 \pm 0.66 \times 10^4$; $P < 0.0001$; HP: $5.72 \pm 0.24 \times 10^4$; $P < 0.0001$, one-way ANOVA with Tukey's post hoc multiple comparisons). *AAV9/hPS1-EGFP* significantly reduces microglia in the neocortex ($37.53 \pm 1.92 \times 10^4$) and hippocampus ($6.75 \pm 0.08 \times 10^4$) of injected *PS* cDKO mice, compared to uninjected (NCX: $P = 0.0121$; HP: $P < 0.0001$). The number of microglia is also significantly elevated in the neocortex ($50.17 \pm 1.64 \times 10^4$; $P < 0.0001$) and hippocampus ($8.04 \pm 0.14 \times 10^4$; $P = 0.0001$) of *Psen1*[L435F/F]; *Psen2*^{−/−}; *Cre* mice, compared to control mice. *AAV9/hPS1-EGFP* also significantly reduces microglia in the neocortex ($36.29 \pm 1.9 \times 10^4$) and hippocampus ($4.85 \pm 0.23 \times 10^4$) of injected *Psen1*[L435F/F]; *Psen2*^{−/−}; *Cre* mice, compared to uninjected ($P < 0.0001$). (*C*) Western analysis of GFAP using cortical lysates of littermate *PS* cDKO, *Psen1*[L435F/F]; *Psen2*^{−/−}; *Cre*, and control mice injected with *AAV9/hPS1-EGFP* or no AAV. (*D*) Quantification of GFAP levels shows marked increases of GFAP in the cortex of *PS* cDKO (N = 5) and *Psen1*[L435F/F]; *Psen2*^{−/−}; *Cre* (N = 6) mice at 10 mo of age, compared to controls (N = 4, $P < 0.0001$). Introduction of *AAV9/hPS1-EGFP* effectively restores GFAP levels in *PS* cDKO mice (N = 7, $P < 0.0001$), and levels of GFAP are similar between *AAV9/hPS1-EGFP*-injected *PS* cDKO mice and control mice ($P = 0.5795$). Similarly, levels of GFAP are elevated in the cortex of *Psen1*[L435F/F]; *Psen2*^{−/−}; *Cre* mice, compared to controls ($P < 0.0001$). *AAV9/hPS1-EGFP* rescues elevated GFAP levels in the cortex of *Psen1*[L435F/F]; *Psen2*^{−/−}; *Cre* mice (N = 8, $P < 0.0001$). All data represent mean ± SEM. *$P < 0.05$, ***$P < 0.001$, ****$P < 0.0001$. Yellow filled and open circles represent data obtained from individual male and female mice, respectively.

in excitatory neurons of the cortex in *PS* cDKO mice. Indeed, GFP immunoreactivity co-localizes with neuronal marker NeuN in the neocortex and hippocampus (*SI Appendix*, Fig. S2), and *AAV9/hPS1-EGFP* but not *AAV9/EGFP* dramatically reduces APP CTF immunoreactivity (*SI Appendix*, Fig. S3). Furthermore, using recombinant γ-secretase substrates of Notch and APP in an in vitro assay, expression of hPS1 by *AAV9/hPS1* also restores production of NICD and Aβ in *Psen* mutant mice (*SI Appendix*, Fig. S4). Importantly, hPS1 or GFP expression from a single delivery of *AAV9/hPS1-EGFP* is sustained over a long period of time, and the restoration of impaired γ-secretase activity is also maintained to aged brains (*SI Appendix*, Figs. S8 and S11). Thus, low to moderate levels of hPS1 are sufficient to rescue impaired γ-secretase activity caused by *Psen* mutations.

**hPS1 Overcomes Dominant Negative Effects of FAD *Psen1* Mutation.** FAD *PSEN1* mutations were reported to act in a dominant negative manner to inhibit γ-secretase activity of the

wild-type *PSEN1* allele using both in vitro biochemical assays and cell culture systems (20, 21, 25, 38). These findings are consistent with the lack of nonsense mutations identified in FAD cases, despite the large number (>400) of mostly missense mutations in *PSEN1* and *PSEN2* (https://www.alzforum.org/mutations). However, PS is the catalytic subunit of the γ-secretase complex composed of 4 protein components present in equal stoichiometric amounts, suggesting that expression of hPS1 may displace mutant mPS1 in the γ-secretase complex. Indeed, we found that expression of hPS1 results in significant decreases of mPS1 CTF in the cortex of *Psen1*[L435F/F]; *Psen2*^{−/−}; *Cre* mice (Fig. 1), providing experimental evidence for the proposed displacement. Furthermore, expression of hPS1, albeit at low to moderate levels, is sufficient to reduce drastically the accumulation of APP CTFs in the cortex of *Psen1*[L435F/F]; *Psen2*^{−/−}; *Cre* mice (Fig. 1 and *SI Appendix*, Figs. S1 and S3). Compared to the normal PS1 expression in nonexcitatory neurons of the cerebral cortex in *PS* cDKO mice, such as inhibitory neurons and glial populations,

PS1 L435F mutant is expressed in all cells of the cerebral cortex of *Psen1*[L435F/F]; *Psen2*^{−/−}; *Cre* mice, which may explain the greater accumulation of APP CTFs in these mice.

hPS1 delivered by AAV9 also reversed the increase of APP CTFs in the cerebral cortex of *Psen1*[L435F/+]; *Psen2*^{−/−} mice and *Psen1*[L435F/+] mice, which are genetically identical to FAD patients carrying the same mutation (Fig. 1 and *SI Appendix*, Fig. S1). L435F abolishes γ-secretase activity in in vitro biochemical systems, culture cells, and KI/KI mice, and L435F KI/KI mice phenotypically resemble germline *Psen1* KO mice (20, 22, 23, 25). The impact of L435F on disruption of PS1 function is independently supported by structural analysis, showing that the L435 residue is located closest to the two aspartate residues at the active site of γ-secretase (26). Not surprisingly, the absence of PS2 results in a greater accumulation of APP CTFs in the cortex of *Psen1*[L435F/F]; *Psen2*^{−/−} mice, compared to *Psen1*[L435F/+] mice (Fig. 1 and *SI Appendix*, Fig. S1). For *Psen1*[L435F/+] mice, the shorter *AAV9/hPS1* achieved the rescue, whereas the longer *AAV9/hPS1-EGFP* was unable to, though we were unable to separate hPS1 from mPS1, due to the lack of specific antibodies. Interestingly, only hPS1 expressed from *AAV9/hPS1*, without the extra 18 amino acid residues attached to hPS1 CTF, was able to cleave recombinant Notch and APP substrates in CHAPSO solubilized membrane preparation. Moreover, hPS1 is expressed under the control of the *hCamk2a* promoter, which targets hPS1 expression in excitatory neurons selectively. Thus, *AAV9/hPS1-EGFP* is unable to rescue impaired γ-secretase activity in nonexcitatory neuron populations in the cerebral cortex, where L435F mutant KI allele is expressed.

**hPS1 Rescues Synaptic and Memory Deficits and Neurodegeneration in *Psen* Mutant Mice.** While biochemical analysis permits quantitative assessment of the reduction of γ-secretase activity in various *Psen* mutant mice and the extent of the rescue by hPS1 delivered by *AAV9/hPS1-EGFP* and *AAV9/hPS1*, it is important to determine if expression of hPS1 rescues functional impairments caused by *Psen* mutations. We found that *AAV9/hPS1-EGFP* reversed synaptic plasticity impairments, such as PPF, synaptic facilitation, and LTP in the hippocampal Schaffer collateral pathway of *PS* cDKO mice (*SI Appendix*, Fig. S5). Moreover, *AAV9/hPS1-EGFP* also improved spatial learning and memory performances of *Psen* mutant mice at the age of 5 mo in the water maze (Fig. 2) despite varying, low to moderate levels of hPS1 in the cortex of individual mutant mice (*SI Appendix*, Fig. S8). Most importantly, hPS1 introduced by AAV9 rescued the loss of cortical neurons in *PS* cDKO mice and *Psen1*[L435F/F]; *Psen2*^{−/−}; *Cre* mice at the age of 10 mo (Fig. 3) even though low to moderate levels of hPS1 were detected in the dissected cortex (Fig. 1 and *SI Appendix*, Fig. S8), suggesting that maintaining normal neuronal integrity and survival during aging does not require normal levels of PS1 expression. Furthermore, hPS1 levels are not diminished at the ages of 6 to 10 mo (*SI Appendix*, Fig. S8). These findings are consistent with earlier reports showing that one functional copy of PS1 but not PS2 is sufficient to prevent neurodegeneration, as indicated by the normal cortical neuron number in *Psen1*[+/F]; *Psen2*^{−/−}; *Cre* mice (22) but not in *Psen1*[F/F]; *Psen2*^{+/−}; *Cre* mice (16). Moreover, elevated microgliosis and astrogliosis in the cerebral cortex of *PS* cDKO and *Psen1*[L435F/F]; *Psen2*^{−/−}; *Cre* mice are also reversed by *AAV9/hPS1-EGFP* (Fig. 4 and *SI Appendix*, Figs. S9 and S10).

In summary, the current study serves as preclinical, proof-of-concept testing of PS-based gene therapy targeting early-onset AD carrying *PSEN* mutations. Our findings demonstrate that even low to moderate levels of hPS1 delivered by AAV9 are sufficient to rescue functional impairments and neurodegeneration associated with *Psen* mutations in the mouse cerebral cortex. The sensitivity of APP CTFs and Aβ peptides to varying γ-secretase activity and the availability of reagents to measure these γ-secretase substrates and products provide valuable biomarkers to assess varying levels of γ-secretase activity. However, many technical challenges remain. For example, the human cerebral cortex is much larger than the mouse cerebral cortex, requiring an AAV capsid capable of broader transduction and distribution by systemic delivery. Recent development of AAV9-derived novel capsids that show robust delivery across the blood–brain barrier, widespread CNS transduction in nonhuman primates following noninvasive intravenous administration hold great promise for gene therapy targeting neurological diseases, such as FAD.

## Materials and Methods

**Mice.** All animal procedures were approved by the Institutional Animal Care and Use Committee at the Brigham and Women's Hospital. The generation and characterization of *PS* cDKO and *Psen1*[L435F/+] mice were previously described (8, 9, 11–14, 22) and were maintained in the C57BL6/129 hybrid background by breeding to wild-type C57BL6/129 F1 mice periodically (three to four generations).

**Generation of AAV Vectors.** Detailed information about the generation of and sequences of pAAV vectors can be found in *SI Appendix*, Fig. S12. All recombinant AAV9 viral particles were produced by UMASS Vector Core as previously reported (39). Briefly, rAV rAAV was produced by using the helper-free triple-plasmid (pAAV plasmids, packing plasmid expressing the AAV serotype 9 capsid, and pAd helper plasmid) transfection method in HEK-293 cells. The rAAV production was followed by purification using cesium chloride (CsCl) gradient sedimentation and ultracentrifugation. The purified rAAVs were tittered by droplet digital PCR, and their purity was determined by silver-stained SDS-PAGE. Intracerebroventricular injections were carried out following a published protocol with modifications (40) and were described in detail in *SI Appendix, Materials and Method*.

**Western, Behavioral, and Histological Analyses.** For the Western analysis, RIPA soluble protein lysates were prepared, and immunoblotting and quantifications were performed as described (22, 35, 37). Antibodies used for Western analysis are described in *SI Appendix, Materials and Methods* and Table S1. The Morris water maze test was performed as described previously (18, 22, 37), and the detailed information can be found in *SI Appendix, Materials and Methods*. Histological analysis was performed as described previously (22, 35, 37, 41), and detailed information can be found in *SI Appendix, Materials and Methods*.

**Data Quantification and Statistical Analysis.** Data acquisition and quantification were performed in a genotype blind manner with the exception of the molecular analysis (Western and in vitro γ-secretase assay). All statistical analysis was performed using Prism (Version 9; GraphPad), Excel (Microsoft), Igor Pro (Version 6.3; Wave-Metrics), or Clampfit (Version 10.3; Molecular device). All data are presented as the mean ± SEM. The exact sample size (e.g., the number of mice or brain slices) of each experiment is indicated in the figure. Statistical analysis was conducted using one-way ANOVA followed up by Tukey's multiple comparisons (Figs. 1–4 and *SI Appendix*, Figs. S1, S4, S5, S9, and S10) or Dunnett's multiple comparisons (*SI Appendix*, Fig. S7), two-way ANOVA followed up by Tukey's multiple comparisons (Fig. 2) or Bonferroni's multiple comparisons (Fig. 2 and *SI Appendix*, Figs. S5 and S6), and unpaired Student's *t*-test (*SI Appendix*, Fig. S6). All statistical comparisons were performed on the data from ≥3 biologically independent samples. Significant is shown as *$P < 0.05$, **$P < 0.01$, ***$P < 0.001$, ****$P < 0.0001$, or NS, not significant.

**Data, Materials, and Software Availability.** All data are included in the manuscript and/or *SI Appendix*.

Author affiliations: [a]Department of Neurology, Brigham and Women's Hospital, Boston, MA 02115; and [b]Program in Neuroscience, Harvard Medical School, Boston, MA 02115

1. E. H. Schroeter *et al.*, A presenilin dimer at the core of the gamma-secretase enzyme: Insights from parallel analysis of Notch 1 and APP proteolysis. *Proc. Natl. Acad. Sci. U.S.A.* **100**, 13075–13080 (2003).
2. J. Shen *et al.*, Skeletal and CNS defects in Presenilin-1-deficient mice. *Cell* **89**, 629–639 (1997).
3. W. Song *et al.*, Proteolytic release and nuclear translocation of Notch-1 are induced by presenilin-1 and impaired by pathogenic presenilin-1 mutations. *Proc. Natl. Acad. Sci. U.S.A.* **96**, 6959–6963 (1999).
4. M. Handler, X. Yang, J. Shen, Presenilin-1 regulates neuronal differentiation during neurogenesis. *Development* **127**, 2593–2606 (2000).
5. M. Wines-Samuelson, J. Shen, Presenilins in the developing, adult, and aging cerebral cortex. *Neuroscientist* **11**, 441–451 (2005).
6. M. Wines-Samuelson, M. Handler, J. Shen, Role of presenilin-1 in cortical lamination and survival of Cajal-Retzius neurons. *Dev. Biol.* **277**, 332–346 (2005).
7. W. Y. Kim, J. Shen, Presenilins are required for maintenance of neural stem cells in the developing brain. *Mol. Neurodegener* **3**, 2 (2008).
8. H. Yu *et al.*, APP processing and synaptic plasticity in presenilin-1 conditional knockout mice. *Neuron* **31**, 713–726 (2001).
9. V. Beglopoulos *et al.*, Reduced beta-amyloid production and increased inflammatory responses in presenilin conditional knock-out mice. *J. Biol. Chem.* **279**, 46907–46914 (2004).
10. R. Feng *et al.*, Forebrain degeneration and ventricle enlargement caused by double knockout of Alzheimer's presenilin-1 and presenilin-2. *Proc. Natl. Acad. Sci. U.S.A.* **101**, 8162–8167 (2004).
11. C. A. Saura *et al.*, Loss of presenilin function causes impairments of memory and synaptic plasticity followed by age-dependent neurodegeneration. *Neuron* **42**, 23–36 (2004).
12. C. Zhang *et al.*, Presenilins are essential for regulating neurotransmitter release. *Nature* **460**, 632–636 (2009).
13. M. Wines-Samuelson *et al.*, Characterization of age-dependent and progressive cortical neuronal degeneration in presenilin conditional mutant mice. *PLoS One* **5**, e10195 (2010).
14. D. Zhang *et al.*, Inactivation of presenilins causes pre-synaptic impairment prior to post-synaptic dysfunction. *J. Neurochem.* **115**, 1215–1221 (2010).
15. B. Wu, H. Yamaguchi, F. A. Lai, J. Shen, Presenilins regulate calcium homeostasis and presynaptic function via ryanodine receptors in hippocampal neurons. *Proc. Natl. Acad. Sci. U.S.A.* **110**, 15091–15096 (2013).
16. H. Watanabe, M. Iqbal, J. Zheng, M. Wines-Samuelson, J. Shen, Partial loss of presenilin impairs age-dependent neuronal survival in the cerebral cortex. *J. Neurosci.* **34**, 15912–15922 (2014).
17. J. Kang, S. Shin, N. Perrimon, J. Shen, An evolutionarily conserved role of presenilin in neuronal protection in the aging Drosophila brain. *Genetics* **206**, 1479–1493 (2017).
18. S. H. Lee *et al.*, Presenilins regulate synaptic plasticity and mitochondrial calcium homeostasis in the hippocampal mossy fiber pathway. *Mol. Neurodegener* **12**, 48 (2017).
19. J. Shen, R. J. Kelleher III, The presenilin hypothesis of Alzheimer's disease: Evidence for a loss-of-function pathogenic mechanism. *Proc. Natl. Acad. Sci. U.S.A.* **104**, 403–409 (2007).
20. E. A. Heilig, W. Xia, J. Shen, R. J. Kelleher III, A presenilin-1 mutation identified in familial Alzheimer disease with cotton wool plaques causes a nearly complete loss of gamma-secretase activity. *J. Biol. Chem.* **285**, 22350–22359 (2010).
21. E. A. Heilig, U. Gutti, T. Tai, J. Shen, R. J. Kelleher III, Trans-dominant negative effects of pathogenic PSEN1 mutations on γ-secretase activity and Aβ production. *J. Neurosci.* **33**, 11606–11617 (2013).
22. D. Xia *et al.*, Presenilin-1 knockin mice reveal loss-of-function mechanism for familial Alzheimer's disease. *Neuron* **85**, 967–981 (2015).
23. D. Xia, R. J. Kelleher III, J. Shen, Loss of Aβ43 production caused by Presenilin-1 mutations in the knockin mouse brain. *Neuron* **90**, 417–422 (2016).
24. L. Sun, R. Zhou, G. Yang, Y. Shi, Analysis of 138 pathogenic mutations in presenilin-1 on the in vitro production of Aβ42 and Aβ40 peptides by γ-secretase. *Proc. Natl. Acad. Sci. U.S.A.* **114**, E476–e485 (2017).
25. R. Zhou, G. Yang, Y. Shi, Dominant negative effect of the loss-of-function γ-secretase mutants on the wild-type enzyme through heterooligomerization. *Proc. Natl. Acad. Sci. U.S.A.* **114**, 12731–12736 (2017).
26. X. C. Bai *et al.*, An atomic structure of human γ-secretase. *Nature* **525**, 212–217 (2015).
27. G. Woodruff *et al.*, The presenilin-1 ΔE9 mutation results in reduced γ-secretase activity, but not total loss of PS1 function, in isogenic human stem cells. *Cell Rep.* **5**, 974–985 (2013).
28. M. L. L. Donnelly *et al.*, Analysis of the aphthovirus 2A/2B polyprotein "cleavage" mechanism indicates not a proteolytic reaction, but a novel translational effect: a putative ribosomal "skip". *J. Gen. Virol.* **82**, 1013–1025 (2001).
29. R. D. Dayton, D. B. Wang, R. L. Klein, The advent of AAV9 expands applications for brain and spinal cord gene delivery. *Expert. Opin. Biol. Ther.* **12**, 757–766 (2012).
30. M. Mayford *et al.*, Control of memory formation through regulated expression of a CaMKII transgene. *Science* **274**, 1678–1683 (1996).
31. H. Watanabe, D. Xia, T. Kanekiyo, R. J. Kelleher III, J. Shen, Familial frontotemporal dementia-associated presenilin-1 c.548G>T mutation causes decreased mRNA expression and reduced presenilin function in knock-in mice. *J. Neurosci.* **32**, 5085–5096 (2012).
32. Y. Takahashi *et al.*, Sulindac sulfide is a noncompetitive gamma-secretase inhibitor that preferentially reduces Abeta 42 generation. *J. Biol. Chem.* **278**, 18664–18670 (2003).
33. S. H. Lee, V. Y. Bolshakov, J. Shen, Presenilins regulate synaptic plasticity in the perforant pathways of the hippocampus. *Mol. Brain* **16**, 17 (2023).
34. G. Huang *et al.*, Motor impairments and dopamingergic defects caused by loss of LRRK function in mice. *J. Neurosci.* **42**, 4755–4765 (2022).
35. J. Kang, J. Shen, Cell-autonomous role of Presenilin in age-dependent survival of cortical interneurons. *Mol. Neurodegener* **15**, 72 (2020).
36. J. Saraiva, R. J. Nobre, L. Pereira de Almeida, Gene therapy for the CNS using AAVs: The impact of systemic delivery by AAV9. *J. Control Release* **241**, 94–109 (2016).
37. S. H. Lee *et al.*, APP family regulates neuronal excitability and synaptic plasticity but not neuronal survival. *Neuron* **108**, 676–690 (2020).
38. H. Watanabe, J. Shen, Dominant negative mechanism of Presenilin-1 mutations in FAD. *Proc. Natl. Acad. Sci. U.S.A.* **114**, 12635–12637 (2017).
39. M. Sena-Esteves, G. Gao, Introducing genes into mammalian cells: Viral vectors. *Cold Spring Harb. Protoc.* **2020**, 095513 (2020).
40. J. Y. Kim, S. D. Grunke, Y. Levites, T. E. Golde, J. L. Jankowsky, Intracerebroventricular viral injection of the neonatal mouse brain for persistent and widespread neuronal transduction. *J. Vis. Exp*, 51863 (2014).
41. J. Kang, H. Watanabe, J. Shen, Protocols for assessing neurodegenerative phenotypes in Alzheimer's mouse models. *STAR Protoc.* **2**, 100654 (2021).